Eur. J. Mineral.
2018, **30**, 1021–1035
Published online 9 May 2018

Lead-antimony sulfosalts from Tuscany (Italy). XXIII. Andreadiniite, $CuAg_7HgPb_7Sb_{24}S_{48}$, a new oversubstituted (Cu,Hg)-rich member of the andorite homeotypic series from the Monte Arsiccio mine, Apuan Alps

Cristian BIAGIONI[1,*], Yves MOËLO[2], Paolo ORLANDI[1] and Werner H. PAAR[3]

[1] Dipartimento di Scienze della Terra, Università di Pisa, Via S. Maria 53, 56126 Pisa, Italy
*Corresponding author, e-mail: cristian.biagioni@unipi.it
[2] Institut des Matériaux Jean Rouxel, UMR 6502, CNRS, Université de Nantes, 2 rue de la Houssinière, 44322 Nantes Cedex 3, France
[3] Department of Chemistry and Physics of Materials, University of Salzburg, Jakob-Haringer-Strasse 2a, 5020 Salzburg, Austria

Abstract: The new mineral species andreadiniite, $CuAg_7HgPb_7Sb_{24}S_{48}$, was discovered in a quartz vein embedded in metadolostone from the Sant'Olga tunnel, Monte Arsiccio mine, Stazzema, Apuan Alps, Tuscany, Italy. It occurs as black anhedral grains, up to some mm in size, with a metallic luster, associated with sphalerite and stibnite. Under the ore microscope, andreadiniite is white, with a slightly yellow-bronze tint. Pleochroism was not observed. Anisotropism is weak, in shades of gray to bluish-gray. Reflectance percentages for the four COM wavelengths are [R_{min}, R_{max} (%), (λ)]: 34.8, 36.4 (470 nm); 33.5, 35.1 (546 nm); 32.9, 35.0 (589 nm); and 31.8, 32.4 (650 nm). Electron-microprobe analysis gave (in wt% – average of seven spot analyses): Cu 1.06(2), Ag 11.25(18), Tl 0.45(9), Hg 2.76 (14), Pb 19.95(16), As 1.55(5), Sb 40.45(21), S 22.23(11), total 99.70(42). On the basis of $\Sigma Me = 40$ atoms per formula unit, the chemical formula is $Cu_{1.14}Ag_{7.12}Tl_{0.15}Hg_{0.94}Pb_{6.57}(Sb_{22.68}As_{1.41})_{\Sigma 24.09}S_{47.33}$, ideally $CuAg_7HgPb_7Sb_{24}S_{48}$. The main diffraction lines, corresponding to multiple *hkl* indices, are [*d* in Å (relative visual intensity)]: 3.719 (ms), 3.406 (s), 3.277 (s), 2.885 (s), 2.740 (ms), 2.131 (ms), 2.055 (s), and 1.788(s). The crystal structure study gave a monoclinic pseudo-orthorhombic unit cell, space group $P2_1/c$, with $a = 19.0982(14)$, $b = 17.0093(11)$, $c = 13.0008(10)$ Å, $\beta = 90.083(4)°$, $V = 4223.3(5)$ Å^3, $Z = 2$. The crystal structure was solved and refined to $R_1 = 0.067$ on the basis of 9756 reflections with $F_o > 4\sigma(F_o)$ and 424 refined parameters. Andreadiniite is a new $^{4,4}L$ homologue belonging to the andorite sub-series of Sb-rich members within the lillianite homologous series. Antimony substituting Pb gives an ideal substitution percentage $n = 106.25\%$. Distribution of minor cations (Hg, Cu, As) is detailed. Mercury may play a critical role for the stabilization of andreadiniite, through a complex substitution rule implying three cation sites: $Pb^{2+} + Sb^{3+} + Ag^{+} \rightarrow Sb^{3+} + Ag^{+} + Hg^{2+}$. Copper is subordinate to the two Hg-rich sites. The name honors Andrea Dini (b. 1966) for his contribution to the knowledge of ore deposits from Tuscany and, in particular, the ore geology and mineralogy of Hg ores from Apuan Alps.

Key-words: andreadiniite; lillianite homologous series; new mineral; lead; copper; silver; mercury; antimony; sulfosalt; crystal structure; Apuan Alps.

1. Introduction

The lillianite homologous series, first defined by Makovicky & Karup-Møller (1977a), is a series of primarily Pb–Bi–Sb–Ag sulfosalts composed by slabs of PbS archetype, cut and unit-cell twinned on $(3\,1\,1)_{PbS}$. Different homologues differ in the thickness of the PbS-like slabs, the homologue number *N* being given by the number of octahedra disposed diagonally across the slabs.

Within the lillianite homologous series, two distinct chemical branches can be recognized, *i.e.* the lillianite branch, represented by predominantly Pb–Bi–Ag sulfosalts, and the andorite branch, formed by predominantly Pb–Sb–Ag species (*e.g.*, Makovicky & Topa, 2014a). This second branch is represented by homeotypes of the $N = 4$ homologue (or $^{4,4}L$ homologue, where *L* stands for "lillianite homologue"). In addition to major Pb, Sb, and Ag, other minor elements can be present, such as Cd, Fe, Mn, Cu, and As; in some localities, Bi can partially replace Sb (*e.g.*, Moëlo *et al.*, 1984, 1989). The study by Moëlo *et al.* (1989) can be considered as a point of departure for the modern systematization of this homeotypic series. Since this work, several additional mineral species have been defined (Table 1). Moreover, some unnamed minerals as well as synthetic compounds related to the andorite series are known.

The occurrence of members of the andorite branch in the hydrothermal ores from Apuan Alps was briefly reported by Orlandi & Dini (2004), who cited the identification of "andorite" from the Buca della Vena mine, in association with pyrite, tetrahedrite, and derbylite in vugs of carbonate veins. Any further crystallographic information is still

https://doi.org/10.1127/ejm/2018/0030-2765 0935-1221/18/0030-2765 $ 6.75
© 2018 E. Schweizerbart'sche Verlagsbuchhandlung, D-70176 Stuttgart
Downloaded from https://pubs.geoscienceworld.org/eurjmin/article-pdf/30/5/1021/4541283/ejm_30_5_1021_1035_biagioni_2765_online.pdf
by University of Arizona user

Table 1. Members of the andorite branch within the lillianite homologous series. Unit-cell parameters are given as A_E (elongation axis, superstructure ~4.25 × n), A_L (layer stacking axis), and A_R (ribbon stacking axis).

Mineral	Chemical formula	A_E (Å)	A_L (Å)	A_R (Å)				V (Å^3)	S.G.	Z	Ref.
$n=2$											
Fizélyite	$Ag_{2.5}Pb_7Sb_{10.5}S_{24}$	8.72	19.28	13.23		90.40 (A_E/A_L)		2225.3	$P2_1/n$	2	[1]
Jasrouxite	$Ag_{5.33}Pb_{1.33}(Sb_{8.33}As_5)_{\Sigma 13.33}S_{24}$	8.29	19.10	19.49	89.73	83.45	89.94	3066	$P-1$	3	[2]
Menchettiite	$Mn_{3.2}Ag_2Pb_{4.8}(Sb_6As_4)_{\Sigma 10}S_{24}$	8.48	19.23	12.63		90.08 (A_E/A_L)		2059.4	$P2_1/n$	2	[3]
Ramdohrite	$Cd_{0.5}Ag_{2.75}Pb_6Sb_{10.75}S_{24}$	8.74	19.31	13.05		90.18 (A_E/A_L)			$P2_1/n$	2	[4]
Uchucchacuaite	$Mn_2Ag_2Pb_6Sb_{10}S_{24}$	8.76	19.36	12.73		90.06 (A_E/A_L)		2158.5	$P2_1/n$	2	[5]
$n=4$											
Andreadiniite	$CuAg_7HgPb_7Sb_{24}S_{48}$	17.01	19.10	13.00		90.08 (A_L/A_R)		4223.3	$P2_1/c$	2	[6]
Arsenquatrandorite	$Ag_{8.8}Pb_{6.4}(Sb_{19.05}As_{5.75})_{\Sigma 24.8}S_{48}$	17.04	19.06	12.91		89.99 (A_L/A_R)		4192.4	$P2_1/c$	2	[7]
Quatrandorite	$Ag_{7.5}Pb_9Sb_{23.5}S_{48}$	17.16	19.17	13.04		90.01 (A_L/A_R)		4289.9	$P2_1/c$	2	[8]
Roshchinite	$(Ag,Cu)_{9.5}Pb_5Sb_{25.5}S_{48}$	16.93	19.05	12.95				4175.4	*Pmna* (?)	2	[9]
$n=6$											
Senandorite	$AgPbSb_3S_6$	25.62	19.16	13.00				6382.7	$Pn2_1a$	24	[10]

[1] Yang *et al.* (2009); [2] Makovicky & Topa (2014b); [3] Bindi *et al.* (2012); [4] Makovicky *et al.* (2013); [5] Yang *et al.* (2011); [6] this work; [7] Topa *et al.* (2013a); [8] Nespolo *et al.* (2012); [9] Spiridonov *et al.* (1990); [10] Sawada *et al.* (1987).

lacking. During the investigation of the sulfosalt mineral assemblages from the Monte Arsiccio mine, an andorite-related species was identified. It showed some chemical peculiarities (minor Cu and exceptional Hg contents) promoting its crystallographic investigation. The crystal structure solution and refinement showed the uniqueness of this phase, representing a new oversubstituted member in the andorite homeotypic series.

The mineral and its name have been approved by the IMA-CNMNC, under the number 2014-049. The holotype specimen is deposited in the mineralogical collection of the Museo di Storia Naturale, Università di Pisa, Via Roma 79, Calci, Pisa (Italy), under catalogue number 19688. The name is in honor of Andrea Dini (b. 1966) for his contribution to the knowledge of the ore geology and mineralogy of the Hg deposits from Apuan Alps (Levigliani and Ripa mines, as well as the Monte Arsiccio ore deposit – Dini *et al.*, 1995; Dini *et al.*, 2001; Biagioni *et al.*, 2013). His studies allowed the understanding of the actual status of "leviglianite" (*i.e.* Zn-rich metacinnabar – Dini, 1995) and the description of the new Hg–Bi sulfosalt grumiplucite (Orlandi *et al.*, 1998). Moreover, Andrea Dini has made important and original contributions to the knowledge of the magmatic activity in the Tuscan Magmatic Province and the related ore deposits (*e.g.*, Dini *et al.*, 2002; Dini, 2003).

This paper reports the description of the occurrence of andreadiniite and its crystal structure, discussing its relationships with the other Sb-rich members of the lillianite homologous series.

2. Occurrence and mineral description

2.1. Occurrence and physical properties

Andreadiniite was collected in a quartz vein embedded in metadolostone from the Sant'Olga tunnel, Monte Arsiccio mine, Stazzema, Apuan Alps, Tuscany, Italy (43°58′16″ N, 10°17′05″ E). The Monte Arsiccio mine exploited a pyrite ± baryte ± iron oxide ore deposit located at the contact between the Paleozoic basement, formed by a metavolcanic-metasiliclastic sequence, and the Triassic metadolostone belonging to the *Grezzoni* Formation. The geological setting of the Monte Arsiccio ore deposit has been reported by previous authors (*e.g.*, Costagliola *et al.*, 1990) and an overview on this kind of ore deposits from Apuan Alps can be found in D'Orazio *et al.* (2017). Within the ore deposit, meter-to-decameter-sized lenses of metadolostone were found during the mining activity. One of them is exposed in the Sant'Olga tunnel and it is the type locality for four mineral species: boscardinite (Orlandi *et al.*, 2012), protochabournéite (Orlandi *et al.*, 2013), arsiccioite (Biagioni *et al.*, 2014a), and mapiquiroite (Biagioni *et al.*, 2014b). Andreadiniite is a further addition to this list.

Andreadiniite was identified in only a limited number of samples. The type material is represented by a quartz vein embedded in the dark gray metadolostone, enriched in microcrystalline pyrite, where andreadiniite forms mm-sized lead-gray compact masses, with a metallic luster. It is brittle, with a conchoidal to uneven fracture (Fig. 1). The Vickers hardness, measured with a load of 25 g, is VHN_{25} = 223 kg/mm^2, ranging between 218 and 229 kg/mm^2, corresponding to a Mohs hardness of ~3.5. Density was not measured, because of the scarcity of homogeneous material; on the basis of the empirical formula (see below), the calculated density is 5.36 g/cm^3. In plane-polarized incident light, andreadiniite is white in colour, with a slight yellow bronze tint. Internal reflections, as well as pleochroism, were not observed. Bireflectance is extremely weak. Between crossed polars, andreadiniite is weakly anisotropic, in shades of gray to bluish-gray. Twinning, revealed by the X-ray study (see below), could not be observed. Reflectance values (WTiC as standard) were measured in air and are given in Table 2 and shown in Fig. 2.

Downloaded from https://pubs.geoscienceworld.org/eurjmin/article-pdf/30/5/1021/4541283/ejm_30_5_1021_1035_biagioni_2765_online.pdf
by University of Arizona user

Fig. 1. Andreadiniite as black metallic masses in quartz vein. Sant'Olga level, Monte Arsiccio mine. Collection Museo di Storia Naturale, University of Pisa. Catalogue number 19688. (Online version in color)

Table 2. Reflectance data (%) for andreadiniite in air.

λ (nm)	R_{min}	R_{max}	λ (nm)	R_{min}	R_{max}
400	35.0	–	560	33.0	34.8
420	35.3	36.4	580	33.1	35.2
440	35.9	36.0	**589**	**32.9**	**35.0**
460	34.7	36.1	600	32.9	34.4
470	**34.8**	**36.4**	620	32.3	33.7
480	35.1	36.6	640	31.9	33.1
500	34.8	36.4	**650**	**31.8**	**32.4**
520	34.3	36.1	660	31.5	32.5
540	33.8	35.3	680	31.6	32.4
546	**33.5**	**35.1**	700	30.9	31.7

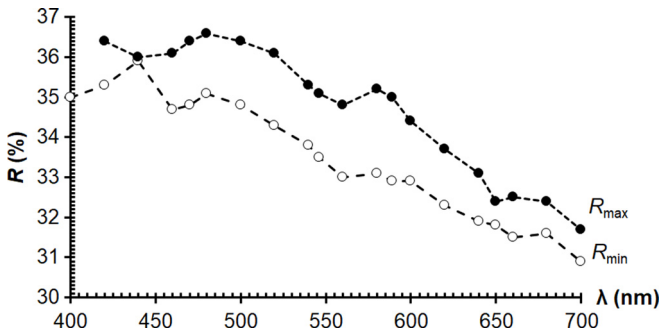

Fig. 2. Reflectance spectra of andreadiniite.

In the type specimen, andreadiniite is associated with sphalerite and stibnite. In the same vein, the thallium sulfosalts boscardinite, protochabournéite, and routhierite were identified, associated with Hg-rich tetrahedrite. The crystallization of this sulfosalt assemblage could be related to the circulation of (Pb, Tl, Ag, Hg, Sb, As)-rich hydrothermal fluids in the fractures of the metadolostone during the Tertiary Alpine tectono-metamorphic events.

2.2. Chemical data

A grain of andreadiniite (sample # 4634) was analyzed with a CAMECA SX50 electron microprobe (BRGM-CNRS-University common laboratory, Orléans, France) operating in WDS mode. The operating conditions were: accelerating voltage 20 kV, beam current 5 nA, beam size 1 μm. Standards (element, emission line, counting times) were: metal Cu (Cu*K*α, 30 s), metal Ag (Ag*L*α, 20 s), HgS (Hg*M*α, 20 s), lorándite (Tl*M*α, 20 s), galena (Pb*M*α, 20 s), stibnite (Sb*L*α, 20 s), AsGa (As*L*α, 30 s), and pyrite (S*K*α, 20 s).

Electron-microprobe data for andreadiniite are given in Table 3. On the basis of $\Sigma Me = 40$ atoms per formula unit (apfu), the chemical formula of andreadiniite can be written as $Cu_{1.14}Ag_{7.12}Tl_{0.15}Hg_{0.94}Pb_{6.57}(Sb_{22.68}\ As_{1.41})_{\Sigma 24.09}S_{47.33}$. After substracting As and Tl according to the substitutions $As^{3+} = Sb^{3+}$ and $Tl^{+} + Sb^{3+} = 2\ Pb^{2+}$, respectively, the formula can be simplified as $Cu_{1.14}Ag_{7.12}Hg_{0.94}Pb_{6.87}Sb_{23.94}S_{47.33}$, ideally $CuAg_7HgPb_7Sb_{24}S_{48}$.

2.3. Crystallography

The X-ray powder diffraction pattern of andreadiniite was collected using a 114.6 mm Gandolfi camera with Ni-filtered Cu*K*α radiation. The observed pattern is reported in Table 4, where it is compared with that calculated using the software *PowderCell* (Kraus & Nolze, 1996) using the structural model described below. Owing to the multiplicity of indices for the majority of the diffraction lines, the unit-cell parameters were not refined.

For the single-crystal X-ray diffraction study, the intensity data were collected using a Bruker Smart Breeze diffractometer with an air-cooled CCD detector, with graphite-monochromatized Mo*K*α radiation. The detector-to-crystal distance was set at 50 mm. A total of 3006 frames was collected using ω and ϕ scan modes in $\Delta\phi = 0.3°$ slices, with an exposure time of 25 s per frame. Data were corrected for Lorentz-polarization factors and absorption using the package of softwares *Apex*2 (Bruker AXS Inc., 2004). The statistical tests on the distribution of $|E|$ values ($|E^2 - 1| = 0.979$) suggested the occurrence of a centre of symmetry. The refined unit-cell parameters are $a = 19.0982(14)$, $b = 17.0093(11)$, $c = 13.0008(10)$ Å, $\beta = 90.083(4)°$, $V = 4223.3(5)$ Å^3, space group $P2_1/c$. The $a:b:c$ ratio is 1.123:1:0.764.

The crystal structure of andreadiniite was refined through *Shelxl*-2014 (Sheldrick, 2015) starting from the atomic coordinates of quatrandorite given by Nespolo *et al.* (2012). Scattering curves for neutral atoms were taken from the *International Tables for Crystallography* (Wilson, 1992). In a first step of the refinement, the scattering curves of Pb, Sb, Ag, and S were used at the Pb, Sb, Ag, and S sites. Several cycles of isotropic refinement led to a high R_1 value (~0.40) that was lowered to a

Downloaded from https://pubs.geoscienceworld.org/eurjmin/article-pdf/30/5/1021/4541283/ejm_30_5_1021_1035_biagioni_2765_online.pdf
by University of Arizona user

Table 3. Electron-microprobe data of andreadiniite: chemical composition (wt%) and chemical formula (in atoms per formula unit, apfu) on the basis of $\Sigma Me = 40$ apfu.

Element	# 4634 ($n = 7$)		
	wt%	range	e.s.d.
Cu	1.06	1.03–1.09	0.02
Ag	11.25	11.05–11.56	0.18
Tl	0.45	0.31–0.58	0.09
Hg	2.76	2.59–2.87	0.14
Pb	19.95	19.76–20.26	0.16
As	1.55	1.51–1.64	0.05
Sb	40.45	40.24–40.81	0.21
S	22.23	22.05–22.42	0.11
Total	99.70	99.10–100.18	0.42

Element	# 4634 ($n = 7$)		
	apfu	range	e.s.d.
Cu	1.14	1.11–1.18	0.02
Ag	7.12	7.00–7.27	0.09
Tl	0.15	0.10–0.19	0.03
Hg	0.94	0.89–1.01	0.04
Pb	6.57	6.52–6.64	0.05
As	1.41	1.38–1.50	0.04
Sb	22.68	22.48–22.82	0.13
S	47.33	46.63–47.63	0.36
Ev *	1.1	0.6–2.2	0.6
$Pb_{corr.}$ **	6.87	6.73–6.97	0.09
$(As + Sb)_{corr.}$ **	23.93	23.73–24.10	0.15

* Relative error on the valence equilibrium (%), calculated as $[\Sigma(val+) - \Sigma(val-)] \times 100/\Sigma(val-)$.
** $Pb_{corr.}$ and $(As + Sb)_{corr.}$ on the basis of the substitution $Tl^{+} + (Sb,As)^{3+} = 2Pb^{2+}$.

Table 4. X-ray powder diffraction data for andreadiniite. Intensities and d_{hkl} were calculated using the software *PowderCell* 2.3 (Kraus & Nolze, 1996) on the basis of the structural model given in Table 6. The eight strongest reflections are given in bold. Only reflections with $I_{calc} \geq 10$ are reported, if not observed. Observed intensities are visually estimated (s = strong; ms = medium-strong; m = medium; mw = medium-weak; w = weak).

I_{obs}	d_{obs}	I_{calc}	d_{calc}	$h\ k\ l$	I_{obs}	d_{obs}	I_{calc}	d_{calc}	$h\ k\ l$
		6	9.55	2 0 0			41	2.739	$\bar{3}$ 4 3
		8	6.15	$\bar{1}$ 0 2	**ms**	**2.740**	42	2.739	3 4 3
		9	6.14	1 0 2	mw	2.382	6	2.387	8 0 0
		9	5.368	$\bar{2}$ 0 2			18	2.262	$\bar{7}$ 4 1
w	5.33	8	5.366	2 0 2	ms	2.263	17	2.261	7 4 1
w	4.04	12	4.044	0 4 1	**ms**	**2.131**	51	2.128	0 8 0
		13	3.846	$\bar{4}$ 0 2			15	2.093	$\bar{3}$ 4 5
mw	3.851	13	3.844	4 0 2	ms	2.092	18	2.093	3 4 5
		39	3.724	$\bar{2}$ 4 1			28	2.056	$\bar{8}$ 4 1
ms	**3.719**	38	3.724	2 4 1	**s**	**2.055**	27	2.055	8 4 1
		60	3.414	$\bar{3}$ 4 1			19	2.010	$\bar{4}$ 4 5
s	**3.406**	66	3.413	3 4 1	m	2.010	23	2.010	4 4 5
		99	3.292	$\bar{5}$ 0 2			11	1.971	$\bar{4}$ 0 6
s	**3.277**	100	3.291	5 0 2	m	1.969	12	1.970	4 0 6
		39	3.245	0 0 4	mw	1.909	16	1.909	10 0 0
		14	3.199	$\bar{1}$ 0 4			9	1.883	$\bar{5}$ 0 6
m	3.199	15	3.199	1 0 4			9	1.882	5 0 6
		10	3.182	6 0 0	ms	1.878	13	1.876	$\bar{8}$ 4 3
		10	3.034	0 4 3			15	1.876	8 4 3
		36	2.997	$\bar{1}$ 4 3			7	1.819	$\bar{6}$ 4 5
m	2.996	36	2.996	1 4 3	mw	1.819	8	1.818	6 4 5
		83	2.892	$\bar{2}$ 4 3			24	1.787	$\bar{5}$ 8 2
s	**2.885**	77	2.891	2 4 3	**s**	**1.788**	14	1.780	5 8 2
		18	2.858	$\bar{6}$ 0 2					
		22	2.857	6 0 2					

reasonable $R_1 = 0.15$ assuming the occurrence of a two-fold twin axis along [1 0 0] [twin ratio 0.50(1)]. Taking into account both the values of the isotropic displacement parameters and the bond lengths, some sites showing a mixed occupancy were detected. Among the four Pb sites, Pb2 and Pb3 showed a mixed (Pb,Sb) occupancy with a splitting between Pb-centered and Sb-centered polyhedra. The refinement of their site occupancy factors (s.o.f.) using the Pb *vs.* Sb scattering curves indicated the occurrence of Sb at Pb1, Pb2, and, in particular, at the Pb3 sites. On the contrary, the Pb4 site was found to be fully occupied by Pb only. The isotropic modeling of the displacement parameters at the Pb3 site was associated with the s.o.f. $Pb_{0.57(1)}Sb_{0.43(1)}$, giving a total amount of Pb agreeing with chemical data, and the U_{iso} value of 0.0275 (4) Å^2. On the contrary, the anisotropic refinement of this atom position resulted in a higher Pb/Sb atomic ratio (*i.e.*, $Pb_{0.83(1)}Sb_{0.17(1)}$) and a definitely higher U_{eq} value (*i.e.*, 0.0492(9) Å^2). Consequently, taking into account the results of the electron-microprobe analysis and the possible occurrence of a larger amount of lighter atoms (*i.e.*, a lower Pb/Sb atomic ratio) suggested by the U_{eq} value, the s.o.f. at the Pb3 position was fixed to $Pb_{0.57}Sb_{0.43}$ and the equivalent isotropic displacement parameter converged to 0.0345(8) Å^2.

The examination of the twelve independent Sb positions showed that Sb6 had a large U_{iso} value and, together with the Sb7 site, bond distances larger than those expected for pure Sb sites. The other sites had U_{iso} and bond lengths agreeing with pure Sb or mixed (Sb,As) occupancies. Consequently, their s.o.f. were refined using the scattering curves of Sb *vs.* As. Refining these sites (but not the Sb6 and Sb7 positions) assuming an anisotropic model, the R_1 lowered to 0.098. The two Sb6 and Sb7 sites were refined assuming a mixed (Sb/Ag) occupancy, and freely refining their atomic coordinates. The R_1 value dropped to 0.089.

Finally, the four independent Ag sites were taken into account. Two of them, corresponding to the Ag2 and Ag3 sites in the structural model proposed for quatrandorite by Nespolo *et al.* (2012), showed definitely shorter *Me*–S distances and high U_{iso}, and were assumed as potential hosts for Cu and Hg. The s.o.f. at these two metal positions, labeled *Me*2 and *Me*3, were refined using the scattering curves of Cu *vs.* Hg, indicating 45.7 and 47.9 electrons in each site, respectively. In addition, the s.o.f. at the Ag1 and Ag4 sites was refined using the scattering curves of Ag *vs.* Hg, indicating a minor replacement of Ag by Hg at these positions. The *Me*2 and *Me*3 sites have large U_{eq} values, possibly indicating a positional disorder related to the different atoms occupying such positions. Actually, whereas it was possible to model two split sub-sites for *Me*2 positions, the *Me*3 site was modeled as an unsplit site, notwithstanding the relatively high U_{eq} value (0.061 Å^2). On the basis of the site scattering values at the *Me*2 and *Me*3 positions, the site populations ($Ag_{0.53}Cu_{0.30}$

Downloaded from https://pubs.geoscienceworld.org/eurjmin/article-pdf/30/5/1021/4541283/ejm_30_5_1021_1035_biagioni_2765_online.pdf
by University of Arizona user

Table 5. Crystal data and summary of parameters describing data collection and refinement for andreadiniite.

Crystal data	
Crystal size (mm)	0.15 × 0.08 × 0.07
Cell setting, space group	Monoclinic, $P2_1/c$
a (Å)	19.0982(14)
b (Å)	17.0093(11)
c (Å)	13.0008(10)
β (°)	90.083(4)
V (Å^3)	4223.3(5)
Z	2
Data collection and refinement	
Radiation, wavelength (Å)	Mo $K\alpha$, λ = 0.71073
Temperature (K)	293
$2\theta_{max}$°	60.13
Measured reflections	51772
Unique reflections	11259
Reflections with $F_o > 4\sigma(F_o)$	9756
R_{int}	0.0372
$R\sigma$	0.0362
Range of h, k, l	$-26 \le h \le 25$, $-23 \le k \le 23$, $-18 \le l \le 18$
R [$F_o > 4\sigma(F_o)$]	0.0672
R (all data)	0.0813
wR (on F_o^2)	0.2329
Goof	1.045
No. of refined parameters	424
Max. and min. residual peak (e·Å^{-3})	6.57 (0.72 Å from Sb10) −3.58 (0.83 Å from Sb12)

$Hg_{0.17}$) and ($Ag_{0.55}Cu_{0.27}Hg_{0.18}$), respectively, could be proposed. They correspond to theoretical site scattering values of 47.2 and 48.1 electrons, respectively.

An anisotropic model for all cations and anions converged to $R_1 = 0.067$ for 9756 reflections with $F_o > 4\sigma(F_o)$ and 424 refined parameters. The chemical formula, obtained through the crystal-structure refinement is $Cu_{1.14}Ag_{6.93}Hg_{0.89}Pb_{6.82}(Sb_{22.84}As_{1.38})_{\Sigma 24.22}S_{48}$ ($Z = 2$). Details of the intensity data collection and crystal-structure refinement are given in Table 5.

3. Crystal-structure description

3.1. General organization

Atomic coordinates, site occupancies, and equivalent isotropic displacement parameters of andreadiniite are given in Table 6, whereas selected bond distances and bond-valence sums for cations, calculated using the bond parameters of Brese & O'Keeffe (1991) are shown in Table 7, deposited and freely available (along with the CIF file) as Supplementary Material linked to this article at https://pubs.geoscienceworld.org/eurjmin/. The unit-cell content of andreadiniite is shown in Fig. 3.

The general organization of andreadiniite, as seen down **b**, is presented in Fig. 4. This mineral is a $N(1,2) = 4,4$ member of the lillianite homologous series. Its crystal structure can be described as formed by the alternation of

Table 6. Atomic coordinates, site occupation factors, and equivalent isotropic displacement parameters (Å^2) for andreadiniite.

Site	s.o.f.	x	y	z	U_{eq}
Pb1	$Pb_{0.93(1)}Sb_{0.07(1)}$	0.24324(5)	0.82630(4)	0.57214(7)	0.0256(3)
Pb2a	$Pb_{0.91(1)}$	0.25351(8)	0.30713(6)	0.59629(12)	0.0379(4)
Sb2b	$Sb_{0.09(1)}$	0.2280(16)	0.3132(12)	0.559(2)	0.0379(4)
Pb3a	$Pb_{0.57}$	0.2536(2)	0.0692(3)	0.5853(4)	0.0345(8)
Sb3b	$Sb_{0.43}$	0.2671(6)	0.0774(8)	0.5689(11)	0.0345(8)
Pb4	$Pb_{1.00}$	0.25073(6)	0.93766(6)	0.08417(10)	0.0424(3)
Sb1	$Sb_{0.89(2)}As_{0.11(2)}$	0.12259(8)	0.69087(7)	0.34350(12)	0.0190(4)
Sb2	$Sb_{0.90(2)}As_{0.10(2)}$	0.95600(7)	0.30308(7)	0.38945(11)	0.0168(4)
Sb3	$Sb_{0.89(2)}As_{0.11(2)}$	0.44830(8)	0.81494(7)	0.12021(10)	0.0159(4)
Sb4	$Sb_{1.00}$	0.44620(8)	0.18511(7)	0.62200(11)	0.0200(3)
Sb5	$Sb_{1.00}$	0.05716(7)	0.32602(7)	0.13436(11)	0.0185(3)
Sb6a	$Sb_{0.65(1)}$	0.3605(3)	0.1901(2)	0.3682(4)	0.0355(10)
Ag6b	$Ag_{0.35(1)}$	0.3702(6)	0.1846(6)	0.3340(9)	0.0355(10)
Sb7a	$Sb_{0.87(2)}$	0.14808(13)	0.0674(2)	0.8704(3)	0.0181(6)
Ag7b	$Ag_{0.13(2)}$	0.1412(8)	0.0496(12)	0.8450(18)	0.0181(6)
Sb8	$Sb_{0.72(2)}As_{0.28(2)}$	0.05928(9)	0.06523(8)	0.11878(12)	0.0180(4)
Sb9	$Sb_{1.00}$	0.37544(8)	0.93582(8)	0.34789(12)	0.0212(3)
Sb10	$Sb_{1.00}$	0.44434(8)	0.92558(8)	0.63047(12)	0.0245(3)
Sb11	$Sb_{0.91(2)}As_{0.09(2)}$	0.04673(7)	0.56193(7)	0.11881(11)	0.0166(4)
Sb12	$Sb_{1.00}$	0.54534(8)	0.94170(8)	0.88283(12)	0.0259(3)
Ag1	$Ag_{0.97(1)}Hg_{0.03(1)}$	0.35780(13)	0.81260(10)	0.8457(2)	0.0432(8)
*Me*2a	$Cu_{0.30}Ag_{0.25}$	0.1472(5)	0.1850(6)	0.3215(5)	0.0382(10)
*Me*2b	$Ag_{0.28}Hg_{0.17}$	0.1339(3)	0.1766(4)	0.3549(4)	0.0382(10)
*Me*3	$Ag_{0.55}Cu_{0.27}Hg_{0.18}$	0.35972(14)	0.05602(13)	0.8296(2)	0.0598(8)
Ag4	$Ag_{0.93(1)}Hg_{0.07(1)}$	0.13127(12)	−0.06206(12)	0.33556(17)	0.0451(8)
S1	$S_{1.00}$	0.3998(3)	0.6978(3)	0.0209(4)	0.0225(10)
S2	$S_{1.00}$	0.0166(3)	0.1998(2)	0.2931(4)	0.0208(9)
S3	$S_{1.00}$	0.1055(3)	0.1682(2)	0.0047(4)	0.0196(9)
S4	$S_{1.00}$	0.1545(3)	0.7935(3)	0.2149(4)	0.0190(9)
S5	$S_{1.00}$	0.0956(2)	0.6490(2)	0.9898(4)	0.0180(9)

Downloaded from https://pubs.geoscienceworld.org/eurjmin/article-pdf/30/5/1021/4541283/ejm_30_5_1021_1035_biagioni_2765_online.pdf
by University of Arizona user

Table 6. (continued).

Site	s.o.f.	*x*	*y*	*z*	U_{eq}
S6	$S_{1.00}$	0.4988(3)	0.8368(3)	0.7593(6)	0.0329(14)
S7	$S_{1.00}$	0.1706(3)	0.3135(3)	0.2236(4)	0.0248(11)
S8	$S_{1.00}$	0.2336(3)	0.6923(3)	0.4318(5)	0.0216(10)
S9	$S_{1.00}$	0.4071(3)	0.2913(3)	0.5095(5)	0.0274(11)
S10	$S_{1.00}$	0.3403(3)	0.1845(3)	0.7235(4)	0.0213(10)
S11	$S_{1.00}$	0.2419(4)	0.1919(3)	0.4439(5)	0.0304(12)
S12	$S_{1.00}$	0.3419(3)	0.8218(3)	0.2357(4)	0.0202(9)
S13	$S_{1.00}$	0.0985(3)	0.9620(2)	0.0064(4)	0.0191(9)
S14	$S_{1.00}$	0.0022(2)	0.4108(2)	0.2671(4)	0.0157(8)
S15	$S_{1.00}$	0.3434(3)	0.0439(3)	0.2215(4)	0.0246(10)
S16	$S_{1.00}$	0.0971(3)	0.4414(3)	0.0268(4)	0.0221(10)
S17	$S_{1.00}$	0.1539(3)	0.5770(3)	0.2315(4)	0.0206(9)
S18	$S_{1.00}$	0.4822(3)	0.0450(3)	0.7878(6)	0.0333(13)
S19	$S_{1.00}$	0.2587(3)	0.9481(3)	0.4276(4)	0.0248(10)
S20	$S_{1.00}$	0.4002(3)	0.9087(3)	−0.0015(4)	0.0209(10)
S21	$S_{1.00}$	0.4019(3)	0.0832(4)	0.5026(4)	0.0268(11)
S22	$S_{1.00}$	0.1613(3)	0.0572(3)	0.2271(4)	0.0240(10)
S23	$S_{1.00}$	0.2656(3)	0.0640(3)	0.9504(5)	0.0265(11)
S24	$S_{1.00}$	0.3310(3)	0.9342(3)	0.7137(4)	0.0226(10)

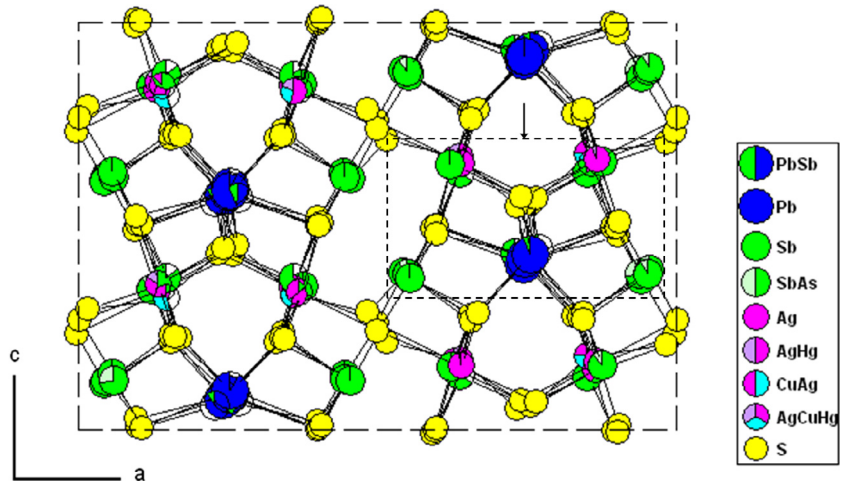

Fig. 3. Unit-cell content of andreadiniite, as seen down **b**. Rectangle: fragment selected for the description of cation ordering along **b** in Fig. 5 (with arrow projection along −**c**). (Online version in color)

$(3\,1\,1)_{PbS}$ slabs, four-octahedra thick along $(1\,0\,0)_{PbS}$ and unit-cell twinned by reflection on $(3\,1\,1)_{PbS}$ planes. The crystal structure of andreadiniite shows a four-fold superstructure with respect to the short 4 Å axis of the substructure and it contains 20 independent cation sites and 24 S sites.

The four independent sites located on the composition planes (1 0 0) of the unit-cell twinning are bicapped trigonal prisms, having a pure Pb occupancy (at the Pb4 position) or mixed (Pb,Sb) populations. Two of them, *i.e.* Pb2 and Pb3, are split into two sub-positions. These sites alternate along **b**, according to the sequence …Pb1–Pb4–Pb2a/Sb2b–Pb3a/Sb3a–Pb1… (Fig. 5).

Two kinds of $(3\,1\,1)_{PbS}$ slabs, each one formed by only one type of diagonal $(1\,0\,0)_{PbS}$ plane, occur in the crystal structure of andreadiniite (Fig. 4). Following Makovicky & Topa (2014b) for the description of the crystal structure of jasrouxite, these two different slabs can be indicated as "central slab" (*C*) and "marginal slab" (*M*), owing to their positions at $y = ½$ (*i.e.*, at a central position within the unit cell) and $y = 0$ and 1 (*i.e.*, at the margins of the unit cell), respectively. The *C* slab is formed by four pure Sb positions (Sb4, Sb9, Sb10, and Sb12), one mixed (Sb,As) site (Sb3), one split (Sb/Ag) position (Sb- and Ag-centered sub-sites labeled as Sb6a and Ag6b, respectively), and two Ag-dominant sites (Ag1 and *Me*3), with possibly a minor replacement of Ag^{+} by Cu^{+} and Hg^{2+}. The *M* slab is composed by one pure Sb position (Sb5), four mixed (Sb, As) sites (Sb1, Sb2, Sb8, and Sb11), one split (Sb/Ag) position (Sb7a and Ag7b), and two Ag-dominant sites (*Me*2 and Ag4), with Ag^{+} partially replaced by Cu^{+} and Hg^{2+}.

Downloaded from https://pubs.geoscienceworld.org/eurjmin/article-pdf/30/5/1021/4541283/ejm_30_5_1021_1035_biagioni_2765_online.pdf
by University of Arizona user

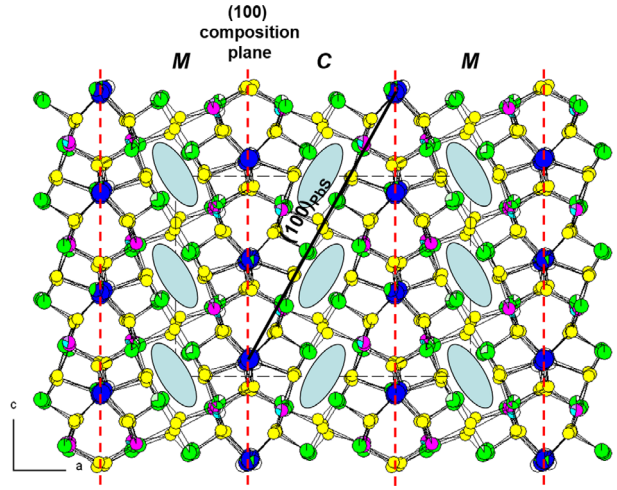

Fig. 4. General organization of andreadiniite, as seen down **b**. The central (*C*) and marginal (*M*) slabs are shown, separated by the (1 0 0) composition planes. Within each slab, $(1\,0\,0)_{PbS}$ atomic layers occur (one of them is shown by the black line). Lone electron-pair micelles are shown as light blue ellipses. (Online version in color)

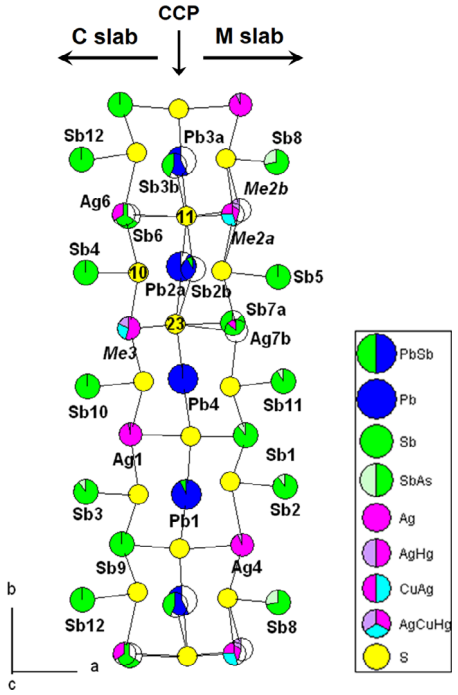

Fig. 5. Cation columns in the *C* (left) and *M* (right) slabs, with the central (1 0 0) composition plane (CCP). (Online version in color)

Every diagonal $(1\,0\,0)_{PbS}$ plane, in both kinds of slabs, is formed by an outer column, flanking the (1 0 0) composition plane, and an inner column, around the lone electron-pair micelle. The *C* slab has outer columns showing the sequence of atom positions, along **b**, …Ag1–*Me*3–Sb6a/Ag6b–Sb9–Ag1…, whereas the inner columns are formed by the sequence …Sb10–Sb4–Sb12–Sb3–Sb10… (Fig. 5). Similarly, in the *M* slab, the sequences …Sb1–Ag4–*Me*2a/*Me*2b–Sb7a/Ag7b–Sb1… and …Sb2–Sb8–Sb5–Sb11–Sb2… represent the outer and inner columns, respectively (Fig. 5). This metal distribution, with Ag occurring in the polyhedra close to or involving the anions of the (1 0 0) composition plane of the unit-cell twinned structure, has been reported in other minerals of the andorite subgroup (*e.g.*, jasrouxite – Makovicky & Topa, 2014b).

3.2. Atom coordinations and site occupancies

In the central (1 0 0) composition plane, the two split sub-sites Pb2a and Pb3a show a bicapped trigonal prismatic coordination, like the pure or Pb-dominant sites Pb4 and Pb1, whereas Sb2b and Sb3b have the typical trigonal pyramidal coordination shown by Sb^{3+}, in an eccentric position, like in jasrouxite (Makovicky & Topa, 2014b), as well as in Pb-rich chabournéite (Biagioni *et al.*, 2015) or boscardinite (Biagioni & Moëlo, 2017a). However, whereas the Sb2b site has three Sb–S distances shorter than 2.70 Å ($\langle$Sb–S$\rangle$ = 2.55 Å), with a bond-valence sum (BVS) of 2.61 valence unit (*v.u.*), the Sb3b position has only one Sb–S distance shorter than 2.70 Å, the other two being 2.72 and 2.87 Å; this results in a severe under-bonding of the Sb atom, likely due to the mean position of neighboring S11 atom. Average $\langle$Pb–S$\rangle$ distances range between 3.118 (Pb3a) and 3.143 Å (Pb1), with Pb–S bond distances ranging from 2.780 (Pb4–S23) to 3.794 Å (Pb1–S12). Bond-valence sums range between 1.89 *v.u.* at the Pb4 site and 2.05 *v.u.* at the split Pb3a position. The minor Tl content (~0.15 apfu) is likely hosted within one of such sites; usually thallium could be attributed to the Pb site having the lowest BVS value, *i.e.* Pb4. However, the difference between the theoretical and observed value at the Pb1 site should be taken into account. Indeed, it has been refined as a mixed $(Pb_{0.93}Sb_{0.07})$ site, with a theoretical BVS of 2.07 *v.u.* Its actual BVS, 1.98 *v.u.*, can be compared with the slight underbonding at Pb4 (1.89 *v.u.*) and consequently it is not possible to propose a reliable hypothesis about the Tl distribution in the crystal structure of andreadiniite.

The ten (Sb,As) sites can be distinguished in pure Sb positions (Sb4, Sb5, Sb9, Sb10, and Sb12) and mixed (Sb, As) sites (Sb1, Sb2, Sb3, Sb8, and Sb11). Taking into account the shortest Me^{3+}–S distances (<2.70 Å – see Moëlo *et al.*, 2012), all these atom positions display the typical trigonal pyramidal coordination, with average Sb–S distances ranging from 2.444 (Sb4) to 2.527 Å (Sb10) for pure Sb positions and from 2.423 (Sb8) to 2.515 Å (Sb2) for mixed (Sb,As) positions. The latter have the highest As content at the Sb8 site, with s.o.f. $(Sb_{0.72}As_{0.28})$. The corresponding BVS values range between 2.80 (Sb2) and 3.36 *v.u.* (Sb4 – its overbonding may be due to mean S10 position).

Two mixed and split (Sb/Ag) positions (Sb6a/Ag6b and Sb7a/Ag7b) were located in the crystal structure of andreadiniite. The Sb-occupied sub-positions display the characteristic three-fold pyramidal coordination, with average bond distances of 2.594 and 2.581 Å at the Sb6a and Sb7a positions. Assuming the full-occupancy of these sites by Sb, the corresponding calculated BVS are 2.70 and 2.90 *v.u.*, respectively. In the split positions Ag6b and Ag7b (Figs. 6a and b), Ag atoms show a distorted

Downloaded from https://pubs.geoscienceworld.org/eurjmin/article-pdf/30/5/1021/4541283/ejm_30_5_1021_1035_biagioni_2765_online.pdf
by University of Arizona user

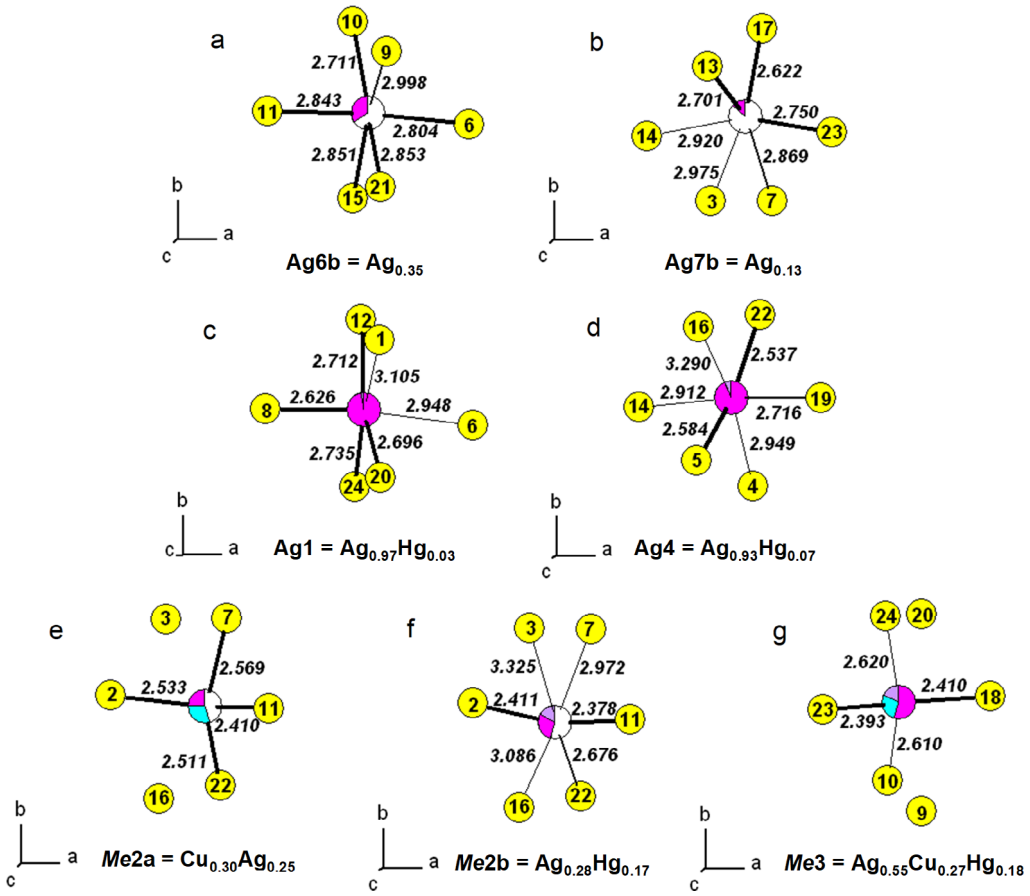

Fig. 6. Coordination of Ag/Cu/Hg-bearing sites in andreadiniite. (Online version in color)

octahedral coordination, with Ag–S distances ranging between 2.62 and 3.00 Å, with average bond distances of 2.843 and 2.806 Å at the Ag6b and Ag7b sites, respectively. The corresponding BVS values are 0.95 and 1.08 *v.u.* for Ag6b and Ag7b.

The four Ag-dominant sites show two distinct kinds of coordination. Ag1 and Ag4 have a distorted octahedral coordination (Figs. 6c and d). Their s.o.f. was modeled assuming a mixed (Ag,Hg) occupancy. Ag1 has only a negligible Hg content ($Hg_{0.03(1)}$), whereas Ag4 has a slightly larger Hg content ($Hg_{0.07(1)}$). Ag1 has four Ag–S distances in the range 2.63–2.73 Å, and two additional longer distances, at 2.95 and 3.10 Å. Its BVS is 1.14 *v.u.* The Ag4 site has a different pattern of bonds. Indeed, it shows three short Ag–S bonds, ranging between 2.54 and 2.72 Å, two longer bonds at 2.91 and 2.95 Å, and a definitely long Ag–S bond at 3.29 Å. The *Me*2 and *Me*3 sites have an Ag-dominant nature, with important substitution of Ag by Cu and Hg. The replacement of Ag by these two metals is well-known in other sulfosalts (*e.g.*, Biagioni *et al.*, 2014c). The *Me*2 site is split into two sub-positions, *Me*2a and *Me*2b (Figs. 6e and f). The former has a distorted tetrahedral coordination, with *Me*–S distances ranging between 2.41 and 2.57 Å; the coordination sphere is completed by two additional longer bonds at 3.54 and 3.56 Å. The latter has two short bonds (2.38 and 2.41 Å) in a linear arrangement (S–*Me*–S angle of 162°), an additional bond at 2.68 Å, and two long bonds at 2.97 and 3.08 Å. The sixth ligand is at 3.33 Å from *Me*2b. Taking into account the refined site scattering and the coordination environment, a mixed (Cu,Ag) population was proposed for the *Me*2a sub-site, whereas a mixed (Ag,Hg) occupancy was hypothesized for the *Me*2b position. Indeed, the distorted octahedral coordination at the *Me*2b sub-site agrees with known Hg coordinations, showing two short opposite bonds and four longer equatorial distances (*e.g.*, rouxelite – Orlandi *et al.*, 2005).

The *Me*3 site has a tetrahedral coordination (Fig. 6g), with two short bonds (2.39 and 2.41 Å), similar to those occurring at the *Me*2b sub-site, two bonds at 2.61–2.62 Å, and two very long *Me*–S bonds at 3.42 and 3.61 Å. The relatively large U_{eq} value could possibly indicate the splitting of this site into two sub-positions, similarly to *Me*2. However, any attempt did not result in an improvement of the crystal-structure refinement. Taking into account the refined site scattering, a mixed (Ag,Cu,Hg) population was hypothesized.

Twenty-four independent S positions have been located in the crystal structure of andreadiniite. Sulfur atoms display tetrahedral (IV), square pyramidal (V), or octahedral (VI) coordinations. The BVS for S atoms (Table 8) range between 1.77 (S1) and 2.29 *v.u.* (S11). The highest BVS (S11, S23) could indicate mean positions between various mixed or split cation sites (Fig. 5).

Downloaded from https://pubs.geoscienceworld.org/eurjmin/article-pdf/30/5/1021/4541283/ejm_30_5_1021_1035_biagioni_2765_online.pdf
by University of Arizona user

Table 8. Bond valence sums (BVS – in valence units) for S atoms in andreadiniite.

Site	BVS	Site	BVS	Site	BVS
S1	1.77	S9	1.95	S17	2.03
S2	2.07	S10	2.04	S18	2.13
S3	2.08	S11	2.29	S19	2.01
S4	2.01	S12	1.98	S20	1.79
S5	1.90	S13	1.91	S21	2.03
S6	2.16	S14	2.07	S22	1.91
S7	1.88	S15	2.02	S23	2.28
S8	2.01	S16	1.89	S24	1.91

4. Crystal chemistry of andreadiniite

4.1. Homologue number and slab composition

The crystal-chemical formula of andreadiniite, as obtained through the refinement of its crystal structure, is $Cu_{1.14}Ag_{6.93}Hg_{0.89}Pb_{6.82}(Sb_{22.84}As_{1.38})_{\Sigma 24.22}S_{48}$ ($Z=2$), with the relative error on the valence equilibrium Ev (%), as defined in the footnote of Table 3, of +0.16. It agrees with the chemical formula obtained through electron-microprobe analysis, $Cu_{1.14}Ag_{7.12}Tl_{0.15}Hg_{0.94}Pb_{6.57}(Sb_{22.68}As_{1.41})_{\Sigma 24.09}S_{47.33}$. Following the calculation procedure for the order N and the $Ag^{+}+Me^{3+}=2Pb^{2+}$ substitution for members of the lillianite homologous series proposed by Makovicky & Karup-Møller (1977a), taking into account minor cations, the homologue order value from chemical analysis is 4.10, close to the crystallographic value $N=4$. Thus, andreadiniite is a $^{4,4}L$ lillianite homologue (Moëlo *et al.*, 2008), with two slabs having the same number of octahedra but distinct chemistry. Indeed, as described above, the crystal structure of andreadiniite can be described as formed by three distinct modules, *i.e.* the (1 0 0) composition plane and the *C* and *M* slabs. These modules have the following chemical compositions, as derived by the crystal structure refinement:

– (1 0 0) composition plane: $[(Pb_{3.41}Sb_{0.59})S_4]^{+0.59}$;
– *C* slab: $[(Ag_{1.52}Cu_{0.27}Hg_{0.21})_{\Sigma 2}(Ag_{0.35}Sb_{5.54}As_{0.11})_{\Sigma 6}S_{10}]^{-0.49}$;
– *M* slab: $[(Ag_{1.46}Cu_{0.30}Hg_{0.24})_{\Sigma 2}(Ag_{0.13}Sb_{5.29}As_{0.58})_{\Sigma 6}S_{10}]^{-0.02}$.

The chemical differences between the two slabs are related to the different As/(As+Sb) atomic ratios. The *C* and *M* slabs have these ratios corresponding to 0.02 and 0.10, respectively, with As being preferentially hosted within the *M* slabs. Likely, these small chemical differences between the two slabs induce the monoclinic symmetry of this species, but with a small β angle, that will favor twinning (observed during the refinement), as well as OD phenomena related to slab stacking.

4.2. Crystal-chemical analysis

The selection of Sb–S short bonds (<2.70 Å – Moëlo *et al.*, 2012) permits to enhance the classic trigonal pyramidal coordination of trivalent Sb. It reveals in the two slabs an infinite –Sb–S– zig-zag chain, corresponding to an Sb_4S_8 periodicity along **b** (Fig. 7). The same chain exists in quatrandorite. The *M* and *C* chains differ only by their As content, a little bit higher in *M* chain: $(Sb_{3.70}As_{0.30})S_8$ (*M*) against $(Sb_{3.89}As_{0.11})S_8$ (*C*). Such small As contents cannot explain the formation of two distinct slabs in andreadiniite.

These chains are completed by isolated groups (Fig. 8). In quatrandorite, it corresponds to Sb_2S_4. In the *C* layer, it corresponds to $Sb(Sb_{0.66}Ag_{0.34})S_4$ and, in the *M* layer, to $(Sb_{0.72}As_{0.28})(Sb_{0.87}Ag_{0.13})S_4$. Taking into account the neighboring cations (see also Fig. 5), it appears that Ag substituting Sb is correlated to Sb substituting Pb: $(Pb3a)^{2+}+(Sb6a)^{3+}\rightarrow(Sb3b)^{3+}+(Ag6b)^{+}$ (*C*) and $(Pb2a)^{2+}+(Sb7a)^{3+}\rightarrow(Sb2b)^{3+}+(Ag7b)^{+}$ (*M*). Such a substitution rule induces a deficit of one positive valence, which is compensated by Hg^{2+} substituting Ag^{+} in two neighboring sites: *Me*2b (*C*), or *Me*3 (*M*). Thus, the whole substitution rule implies three cation sites: $Pb^{2+}+Sb^{3+}+Ag^{+}\rightarrow Sb^{3+}+Ag^{+}+Hg^{2+}$. The oversubstitution in andreadiniite, *i.e.* the replacement of Pb^{2+} by Sb^{3+} in the (1 0 0) composition plane, is correlated to the incorporation of Hg^{2+} within the layers. This justifies to consider Hg as a minor, but essential constituent of this sulfosalt (like Hg in rouxelite – Orlandi *et al.*, 2005). The lower size of Hg^{2+} relatively to Ag^{+} (*Me*–S bond distances: 2.58 *versus* 2.66 Å in tetrahedral coordination) would explain the concentration of smaller Cu^{+} (2.37 Å) on Hg-rich positions. However, it is not possible to prove that Cu acts as an essential constituent.

Due to its lower size and asymmetric triangular pyramidal coordination, Sb3b substituting Pb3b is shifted towards the *M* layer: it is the fundamental factor which governs the crystal-chemical differentiation between the *M* and *C* layers. Minor Sb1 and Sb2b substituting Pb1 and Pb2a, respectively, may be related to OD phenomena (twinning and layer stacking disorder), as well as minor Ag7b (with Sb7a), and Hg substituting Ag1 and Ag4. Ideally, one would have s.o.f. 0.50/0.50 for Pb3a/Sb3b and Sb6/Ag6, and all Hg (s.o.f. sum 0.50) quite equally shared between *Me*2b and *Me*3. Similarly, Cu could be equally shared (in a 0.25/0.25 ratio) between *Me*2a and *Me*3. On this basis, the ideal modular formula of andreadiniite would be $(Pb_{3.5}Sb_{0.5})$ – *M* layer – $(Sb_{0.5}Pb_{3.5})$ – *C* layer, *i.e.* $(Pb_{3.5}Sb_{0.5})S_4$–$[(Sb,As)_{11}Ag_3(AgHg_{0.5}Cu_{0.5})]S_{20}$–$(Pb_{3.5}Sb_{0.5})S_4$–$[(Sb,As)_{12}Ag_2(AgHg_{0.5}Cu_{0.5})]S_{20}$.

4.3. Chemical peculiarities of andreadiniite

Andreadiniite shows some chemical peculiarities with respect to the classic compositional field of members of the andorite homeotypic series:

– Cu content is notable (1.06 wt%), among the highest encountered so far. The occurrence of this monovalent cation has been reported in previous studies. Mozgova *et al.* (1983) give 0.97 wt% Cu in andorite from Baia Sprie (Romania). Moëlo *et al.* (1989) indicate up to 1.11 wt% Cu in a sample from Chazelles-Le Ceroux (Haute-Loire, France), and 1.3 wt% Cu in a sample from

Downloaded from https://pubs.geoscienceworld.org/eurjmin/article-pdf/30/5/1021/4541283/ejm_30_5_1021_1035_biagioni_2765_online.pdf
by University of Arizona user

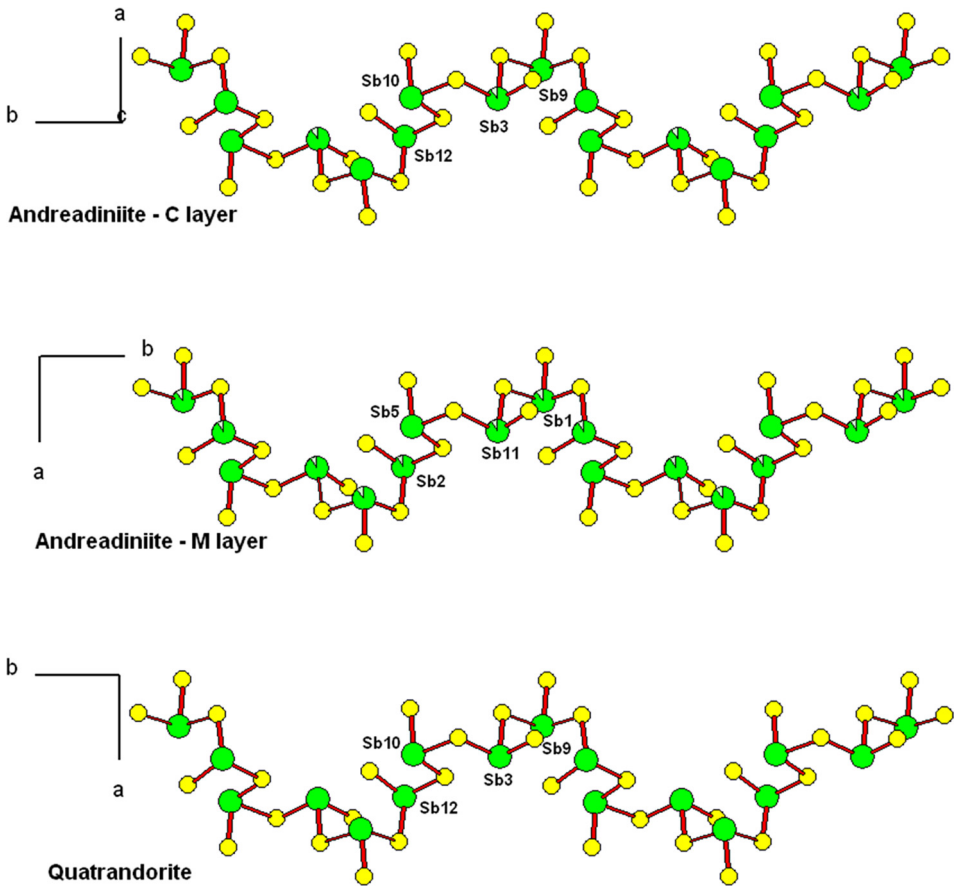

Fig. 7. –Sb–S– zigzag chains with Sb_4S_8 periodicity in *C* and *M* layers of andreadiniite, and in quatrandorite. (Online version in color)

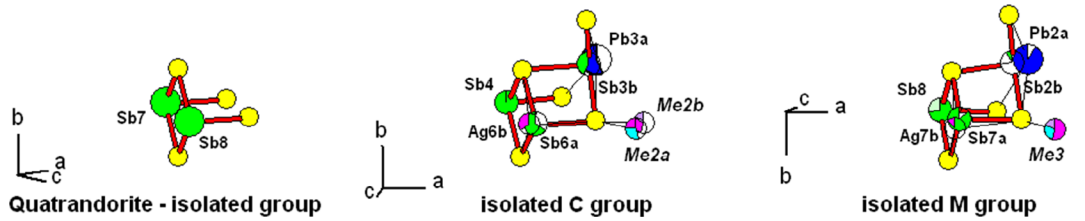

Fig. 8. Sb_2S_4 isolated group in quatrandorite, and its derivatives in *C* and *M* layers of andreadiniite. (Online version in color)

El Mechero mine (Perù), in close intergrowth with a Mn-rich derivative (2.1 wt% Mn). Roshchinite contains up to 0.94 wt% Cu (Spiridonov *et al.*, 1990; Makovicky *et al.*, 2018a);

– Hg content is remarkable. Up to now, Hg was reported only in roshchinite (up to 0.77 wt% – Spiridonov *et al.*, 1990). Its occurrence at Monte Arsiccio agrees with the Hg-rich nature of several sulfides and sulfosalts occurring in the ore assemblages;
– the Tl content is small but significant and it was not reported in previous analyses. The presence of Tl-bearing varieties of non-essential Tl minerals is a characteristic of the Monte Arsiccio ore deposit, *e.g.*, rouxelite and chovanite (Biagioni *et al.*, 2014c, 2017b);
– the As content is relatively high. Higher As contents were reported by Moëlo *et al.* (1989) from two Peruvian deposits (up to 4.5 wt%) and from Jas Roux (France), where Mantienne (1974) first noted the occurrence of the As-to-Sb substitution (As = 2.6 wt%). Recently, three As-rich members of the andorite series have been described, *i.e.* menchettiite (As = 9.27 wt% – Bindi *et al.*, 2012), arsenquatrandorite (ideal As content = 6.56 wt% – Topa *et al.*, 2013a), and jasrouxite (As = 12.77 wt% – Topa *et al.*, 2013b).

4.4. Andreadiniite within the andorite homeotypic series

The simplified chemical formula of the members of the andorite group is $Ag_xPb_{3-2x}Sb_{2+x}S_6$. Within this series, the classification of the minerals can be indicated by the percentage of the andorite component And_n, where n (%) = $100x$. In andreadiniite, ideally $Ag_{8.5}Pb_7Sb_{24.5}S_{48}$, n = 106.25 (107.1 if one takes into account the empirical formula).

Downloaded from https://pubs.geoscienceworld.org/eurjmin/article-pdf/30/5/1021/4541283/ejm_30_5_1021_1035_biagioni_2765_online.pdf
by University of Arizona user

Table 9. Elongation sub-parameter A_E, ribbon corrected parameter A_{Rcorr}, and layer parameter A_L (in Å) in members of the $^{4,4}L$ lillianite homologous series.

	A_E	A_{Rcorr}	A_L	Ref.		A_E	A_{Rcorr}	A_L	Ref.
Bi-rich compounds									
$Sn_3Bi_2S_6$	4.162	13.64	21.21	[1]	$AgPbBi_3S_6$	4.077	13.48	19.88	[9]
$Pb_3Bi_2S_6$	4.110	13.52	20.61	[2]	Gustavite	4.110	13.55	19.45	[10]
	4.120	13.53	20.61	[3]		4.136	13.53	19.57	[11]
Lillianite	4.104	13.54	20.45	[4]		4.111	13.51	19.69	[12]
	4.122	13.57	20.66	[5]	Clino-oscarkempffite	4.140	13.19	19.28	[13]
	4.115	13.53	20.63	[6]	Oscarkempffite	4.145	13.20	19.33	[14]
Xilingolite	4.085	13.50	20.65	[7]	Terrywallaceite	4.194	13.31	19.35	[15]
Sb-rich gustavite	4.171	13.44	19.53	[8]					
Sb-rich compounds									
$LiPbSb_3S_6$	4.197	13.12	19.79	[16]	$Ag_{1.2}Sn_{0.9}Sb_3S_6$ ("Sn-andorite")	4.220	12.89	19.15	[25]
Fizélyite	4.36	13.14	19.23	[17]	$AgPbSb_3S_6$	4.290	13.04	19.17	[25]
	4.354	13.16	19.26	[18]	"Andorite-Bi"	4.280	12.92	19.06	[26]
	4.340	13.21	19.27	[19]	"Andorite-As"	4.248	12.78	19.24	[27]
	4.360	13.23	19.28	[20]	Andreadiniite	4.253	13.00	19.10	[28]
"Ramdohrite"	4.290	12.99	19.21	[17]	Arsenquatrandorite	4.260	12.91	19.06	[29]
Ramdohrite ?	4.360	12.64	19.23	[17]	Quatrandorite	4.268	13.04	19.18	[19]
Ramdohrite-(Fe,Mn)	4.350	12.62	19.20	[19]		4.290	13.04	19.17	[30]
Ramdohrite	4.365	13.09	19.24	[19]	Roshchinite	4.233	12.95	19.05	[31]
	4.370	13.05	19.31	[21]	"Nakaséite"	4.260	13.02	19.18	[32]
Jasrouxite	4.146	12.99	19.10	[22]	Senandorite	4.300	13.00	19.15	[33]
"Andorite"	4.260	12.98	19.15	[17]		4.270	13.00	19.16	[34]
	4.290	13.03	19.15	[23]		4.265	13.01	19.19	[19]
	4.246	13.00	19.17	[24]	$AgMnSb_3S_6$	4.000	12.79	19.58	[35]
	4.303	12.99	19.15	[18]	Menchettiite	4.240	12.63	19.23	[36]
					Uchucchacuaite	4.380	12.73	19.36	[37]

[1] Chen & Lee (2010); [2] Otto & Strunz (1968); [3] Sugaki *et al.* (1974); [4] Takagi & Takéuchi (1972); [5] Pinto *et al.* (2006); [6] Olsen *et al.* (2008); [7] Berlepsch *et al.* (2001); [8] Pažout & Dušek (2009); [9] Bente *et al.* (1993); [10] Karup-Møller (1970); [11] Harris & Chen (1975); [12] Makovicky & Topa (2011); [13] Makovicky *et al.* (2018b); [14] Topa *et al.* (2016); [15] Yang *et al.* (2013); [16] Agha *et al.* (2014); [17] Nuffield (1945); [18] Kašpar *et al.* (1983); [19] Moëlo *et al.* (1989); [20] Yang *et al.* (2009); [21] Makovicky *et al.* (2013); [22] Makovicky & Topa (2014b); [23] Donnay & Donnay (1954); [24] Organova *et al.* (1982); [25] Chang (1987); [26] Mozgova *et al.* (1987); [27] Mantienne (1974); [28] this work; [29] Topa *et al.* (2013a); [30] Nespolo *et al.* (2012); [31] Spiridonov *et al.* (1990); [32] Ito & Muraoka (1960); [33] Kawada & Hellner (1971); [34] Sawada *et al.* (1987); [35] Liu & Chang (1994); [36] Bindi *et al.* (2012); [37] Yang *et al.* (2011).

In the andorite homeotypic series, on the basis of S = 96 atoms, mineral species have composition close to integer values of m in the general formula $Ag_{16-m}Pb_{16+2m}Sb_{48-m}S_{96}$, where $m = 16 \times [1 - (n/100)]$ For instance, taking into account Moëlo *et al.* (1989) and Makovicky & Topa (2014b), one has the following ideal substitution percentages for andorite homeotypes:

– uchucchacuaite and menchettiite: $m \sim 8 \rightarrow And_{50}$;
– fizélyite: $m \sim 6 \rightarrow And_{62.5}$;
– ramdohrite: $m \sim 5 \rightarrow And_{68.75}$;
– quatrandorite: $m \sim 1 \rightarrow And_{93.75}$;
– senandorite: $m \sim 0 \rightarrow And_{100}$;
– arsenquatrandorite: $m \sim -2 \rightarrow And_{112.5}$;
– roshchinite: $m \sim -3 \rightarrow And_{118.75}$
– jasrouxite: $m \sim -5 \rightarrow And_{131.25}$.

For andreadiniite, the n value (107.1) is close to the ideal value corresponding to $m = -1$, *i.e.* $And_{106.25}$, with ideal formula $Ag_{17}Pb_{14}Sb_{49}S_{96}$, *i.e.* $Ag_{8.5}Pb_7Sb_{24.5}S_{48}$ ($Z = 2$). It thus corresponds to a new member in the sequence.

Homeotypes with n values greater than 100% (*i.e.*, $x > 1$) correspond to the so-called "oversubstituted" andorite derivatives, where $(2x - 1)$ Pb is replaced by Sb. Despite the same superstructure (4×) along the 4.25 Å axis, andreadiniite is distinct from quatrandorite, which is "undersubstituted" ($And_{93.75}$) and presents an immiscibility gap with the intermediate member senandorite (And_{100}). Andreadiniite is a close homeotype (same supercell and same space group) of arsenquatrandorite (Topa *et al.*, 2013a), an As-rich oversubstituted andorite member (~$And_{112.5}$). Nevertheless, andreadiniite is As-poor; moreover, Hg substituting Ag clearly favors its stabilization, while the stabilization role of Cu is questionable. Andreadiniite has an oversubstitution value close to that of "nakaséite" ($And_{107.2}$ – Ito & Muraoka, 1960), an oversubstituted andorite that corresponds to a disordered intergrowth of two members with four-fold and six-fold superstructures (Moëlo *et al.*, 1989).

4.5. Sb- *versus* Bi-rich members of the $^{4,4}L$ homologue type

Following the approach developed in previous studies (*e.g.*, Bi-rich members: Makovicky & Karup-Møller, 1977b;

Downloaded from https://pubs.geoscienceworld.org/eurjmin/article-pdf/30/5/1021/4541283/ejm_30_5_1021_1035_biagioni_2765_online.pdf
by University of Arizona user

Sb-rich member: Moëlo *et al.*, 1989), it is interesting to compare andreadiniite to the other members of the $^{4,4}L$ lillianite homologous series on the basis of the unit-cell parameters of their common sub-cells. Table 9 gives the following three values for 47 minerals and synthetic compounds: (i) the elongation sub-parameter A_E (around 4.2 Å), (ii) the layer parameter A_L (around 20 Å), and (iii) the ribbon parameter $A_{Rcorr} = (A_R \times \sin\beta)$ (around 13 Å), taking into account the high obliquity of some species, having β close to 107–108° [for instance gustavite: $A_{Rcorr} = 2d_{(100)}$]. Through the combination of two of these parameters, three diagrams have been obtained (Fig. 9).

Figure 9a shows the relationships between A_L and A_{Rcorr}. There is a regular increase of the two parameters for the compounds of the Ag–Pb–(Sb,As,Bi) sub-system, from arsenquatrandorite to gustavite. One anomaly is represented by "andorite-As" from Jas Roux, owing to its high As content On the contrary, the Pb-Bi rich compounds (lillianite and xilingolite) show a significant A_L increase with a relatively constant A_{Rcorr} parameter, relatively to gustavite.

The relationships between A_E and A_{Rcorr} are shown in Fig. 9b, where four distinct areas can be identified. Two main areas correspond to the andorite sub-group on one hand and, on the other hand, to Bi-rich compounds. Jasrouxite and synthetic $LiPbSb_3S_6$ have an intermediate position. Fizélyite and ramdohrite occupy a restricted area. The fourth area has been delimited to join Mn-rich compounds. Curiously, ramdohrite from the type locality (Sud-Chichas, Potosi, Bolivia), as characterized by Nuffield (1945), belongs to this field and not to the fizélyite–ramdohrite field. It is very close to "ramdohrite-(Fe,Mn)" of Moëlo *et al.* (1989) (see also Fig. 9a). Clearly, the sample of ramdohrite examined by Nuffield (1945) is distinct from ramdohrite studied by Makovicky *et al.* (2013) and could correspond to a distinct mineral species, having a specific name. A careful re-examination of a type specimen of ramdohrite, collecting new electron-microprobe data as well as single-crystal X-ray diffraction data, would be necessary, to check its possible heterogeneity, looking for the occurrence of small minor cation(s) explaining the shorter A_R parameter.

The A_E and A_L parameters are compared in Fig. 9c. A regular distribution of compounds along two branches (Sb- *versus* Bi-rich species) joining within a crescent, from uchucchacuaite (long A_E, short A_L) to lillianite–xilingolite (short A_E, long A_L), occurs. Mixed (Sb/Bi) species are at the junction of these two trends. Only three exotic synthetics, *i.e.* $LiPbSb_3S_6$, $AgMnSb_3S_6$, and $Sn_3Bi_2Se_6$, are outside this area.

These three figures indicate a distinct crystal-chemical role between (Sb,As)- and Bi-rich compounds. Antimony, together with As, favors the elongation of the structures, with an A_E sub-parameter longer than the (1 1 0) periodicity of galena (4.196 Å); on the contrary, Bi favors an increase of the length of the two other sub-parameters, especially A_L. This opposition is the most marked for the highest contents of divalent cations (Pb, Mn, Sn): fizélyite–ramdohrite and uchucchacuaite on the one hand (A_E = 4.34–4.38 Å, A_L = 19.23–19.36 Å), and, on the other hand, lillianite–xilingolite (A_E = 4.12–4.09 Å, A_L = 20.45–20.66 Å). It is the consequence of the more pronounced lone-electron-pair stereo-chemical activity of Sb^{3+} relatively to Bi^{3+}.

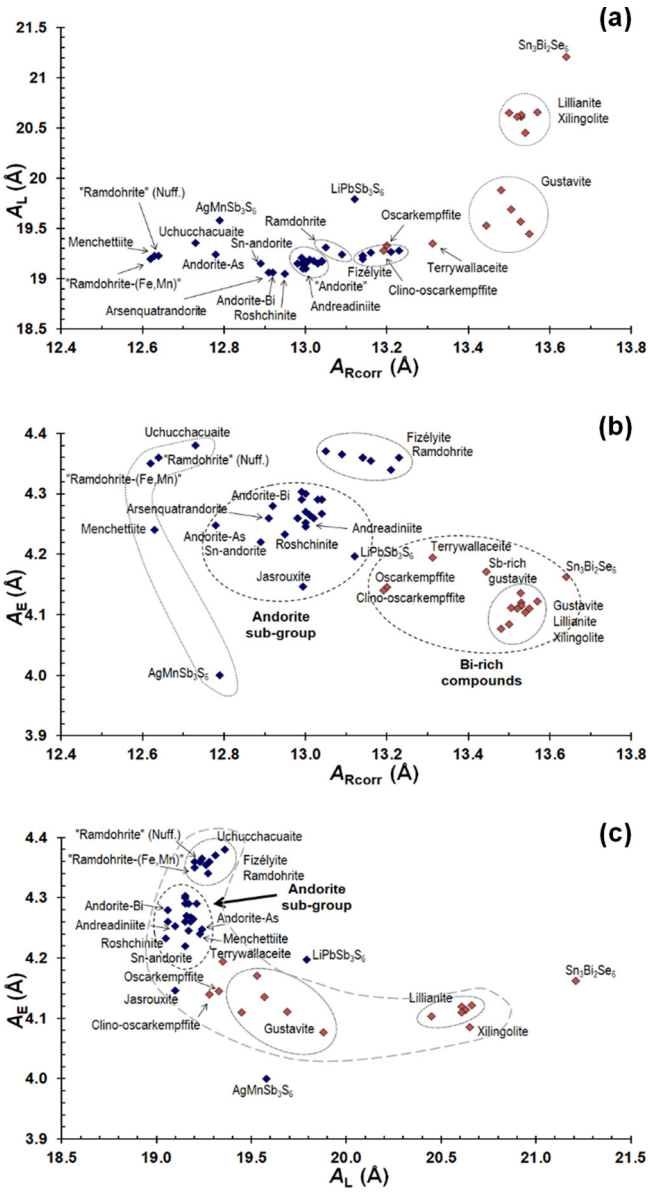

Fig. 9. Relationships between A_E, A_L, and A_{Rcorr} parameters in members of the $^{4,4}L$ lillianite homologous series. (Online version in color)

5. Conclusion

Andreadiniite is a new $^{4,4}L$ oversubstituted member of the andorite series. Its complex crystal chemistry brings new data useful for the knowledge of the lillianite homologous

Downloaded from https://pubs.geoscienceworld.org/eurjmin/article-pdf/30/5/1021/4541283/ejm_30_5_1021_1035_biagioni_2765_online.pdf
by University of Arizona user

series and reveals the critical role played by Hg, in relationship with the oversubstitution due to Sb, for the stabilization of this new species.

This study confirms the close relationships between the minor components occurring in sulfosalts and the geochemistry of the ore bodies. Indeed, andreadiniite has a very intriguing chemical composition, showing the occurrence, together with major Ag, Pb, and Sb, of minor Cu, Hg, Tl, and As. In this way, it mirrors the geochemical complexity of the Monte Arsiccio ore deposit. Indeed, the occurrence of Hg, Tl, and As within a member of the andorite series agrees with the (Hg,Tl,As)-rich nature of the Monte Arsiccio ores, and is in accord with previous studies showing the unusual occurrence of these elements in virtually (Pb/Sb)-pure sulfosalts, *e.g.*, chovanite (Biagioni & Moëlo, 2017b).

Acknowledgments: Riccardo Mazzanti is thanked for providing us with the first specimen of andreadiniite. The constructive comments by Emil Makovicky and Chris J. Stanley were greatly appreciated. This research received support by Ministero dell'Istruzione, dell'Università e della Ricerca through the project SIR 2014 "THALMIGEN – Thallium: Mineralogy, Geochemistry, and Environmental Hazards" (Grant No. RBSI14A1CV), granted to CB.

References

Agha, E.C., Malliakas, C.D., Im, J., Jin, H., Zhao, L.-D., Freeman, A.J., Kanatzidis, M.G. (2014): $LiPbSb_3S_6$: A semiconducting sulfosalt with very low thermal conductivity. *Inorg. Chem.*, **53**, 673–675.

Bente, K., Engel, M., Steins, M. (1993): Crystal structure of lead bismuth silver sulfide. *Z. Kristallogr.*, **205**, 327–328.

Berlepsch, P., Armbruster, T., Makovicky, E., Hejny, C., Topa, D., Graeser, S. (2001): The crystal structure of (0 0 1) twinned xilingolite, $Pb_3Bi_2S_6$, from Mittal-Hohtenn, Valais, Switzerland. *Can. Mineral.*, **39**, 1653–1663.

Biagioni, C. & Moëlo, Y. (2017a): Lead-antimony sulfosalts from Tuscany (Italy). XVIII. New data on the crystal-chemistry of boscardinite. *Mineral. Mag.*, **81**, 47–60.

—, — (2017b): Lead-antimony sulfosalts from Tuscany (Italy). XIX. Crystal chemistry of chovanite from two new occurrences in the Apuan Alps and its 8 Å crystal structure. *Mineral. Mag.*, **81**, 811–831.

Biagioni, C., D'Orazio, M., Vezzoni, S., Dini, A., Orlandi, P. (2013): Mobilization of Tl-Hg-As-Sb-(Ag,Cu)-Pb sulfosalt melts during low-grade metamorphism in the Alpi Apuane (Tuscany, Italy). *Geology*, **41**, 747–750.

Biagioni, C., Bonaccorsi, E., Moëlo, Y., Orlandi, P., Bindi, L., D'Orazio, M., Vezzoni, S. (2014a): Mercury-arsenic sulfosalts from the Apuan Alps (Tuscany, Italy). II. Arsiccioite, $AgHg_2TlAs_2S_6$, a new mineral from the Monte Arsiccio mine: occurrence, crystal structure and crystal chemistry of the routhierite isotypic series. *Mineral. Mag.*, **78**, 101–117.

Biagioni, C., Orlandi, P., Pasero, M., Nestola, F., Bindi, L. (2014b): Mapiquiroite, $(Sr,Pb)(U,Y)Fe_2(Ti,Fe^{3+})_{18}O_{38}$, a new member of the crichtonite group from the Apuan Alps, Tuscany, Italy. *Eur. J. Mineral.*, **26**, 427–437.

Biagioni, C., Moëlo, Y., Orlandi, P. (2014c): Lead-antimony sulfosalts from Tuscany (Italy). XV. (Tl-Ag)-bearing rouxelite from Monte Arsiccio mine: occurrence and crystal chemistry. *Mineral. Mag.*, **78**, 651–661.

Biagioni, C., Moëlo, Y., Favreau, G., Bourgoin, V., Boulliard, J.-C. (2015): Structure of Pb-rich chabournéite from Jas Roux, France. *Acta Crystallogr.*, **B71**, 81–88.

Bindi, L., Keutsch, F.N., Bonazzi, P. (2012): Menchettiite, $AgPb_{2.40}Mn_{1.60}Sb_3As_2S_{12}$, a new sulfosalt belonging to the lillianite series from the Uchucchacua polymetallic deposit, Lima Department, Peru. *Am. Mineral.*, **97**, 440–446.

Brese, N.E., O'Keeffe, M. (1991): Bond-valence parameters for solids. *Acta Crystallogr.*, **B47**, 192–197.

Bruker AXS Inc. (2004): APEX 2. Bruker Advanced X-ray Solutions, Madison, Wisconsin, USA.

Chang, L.L.Y. (1987): $Ag_{1.2}Sn_{0.9}Sb_3S_6$, a tin-bearing andorite phase. *Mineral. Mag.*, **51**, 741–743.

Chen, K.B. & Lee, C.S. (2010): Experimental and theoretical studies of $Sn_{3-\delta}Pb_\delta Bi_2Se_6$ ($\delta = 0/0.07$). *J. Sol. Stat. Chem.*, **183**, 807–813.

Costagliola, P., Benvenuti, M., Tanelli, G., Cortecci, G., Lattanzi, P. (1990): The barite-pyrite-iron oxides deposit of Monte Arsiccio (Apuane Alps). Geological setting, mineralogy, fluid inclusions, stable isotopes and genesis. *Boll. Soc. Geol. Ital.*, **109**, 267–277.

Dini, A. (1995): Metacinabro zincifero ("leviglianite") e sfalerite mercurifera della miniera di Levigliani (Alpi Apuane, Toscana). *Atti Soc. Tosc. Sci. Nat., Mem.*, **102**, 67–71.

— (2003): Ore deposits, industrial minerals and geothermal resources. *Per. Mineral.*, **72**, 41–52.

Dini, A., Benvenuti, M., Lattanzi, P., Tanelli, G. (1995): Mineral assemblages in the Hg-Zn-(Fe)-S system at Levigliani, Tuscany, Italy. *Eur. J. Mineral.*, **7**, 417–427.

Dini, A., Benvenuti, M., Costagliola, P., Lattanzi, P. (2001): Mercury deposits in metamorphic settings: the example of Ripa and Levigliani mines, Apuane Alps (Tuscany, Italy). *Ore Geol. Rev.*, **18**, 149–167.

Dini, A., Innocenti, F., Rocchi, S., Tonarini, S., Westerman, D.S. (2002): The magmatic evolution of the late Miocene laccolith-pluton-dyke granitic complex of Elba Island, Italy. *Geol. Mag.*, **139**, 257–279.

Donnay, J.D.H. & Donnay, G. (1954): Syntaxic intergrowths in the andorite series. *Am. Mineral.*, **39**, 161–171.

D'Orazio, M., Biagioni, C., Dini, A., Vezzoni, S. (2017): Thallium-rich pyrite ores from the Apuan Alps, Tuscany, Italy: constraints for their origin and environmental concerns. *Miner. Deposita*, **52**, 687–707.

Harris, D.C. & Chen, T.T. (1975): Gustavite: two Canadian occurrences. *Can. Mineral.*, **13**, 411–414.

Ito, T. & Muraoka, H. (1960): Nakaséite, an andorite-like new mineral. *Z. Kristallogr.*, **113**, 94–98.

Karup-Møller, S. (1970): Gustavite, a new sulphosalt mineral from Greenland. *Can. Mineral.*, **10**, 173–190.

Kašpar, P., Mrázek, Z., Řídkošil, T. (1983): Andorite, fizelyite and miargyrite: a decomposition of a natural solid solution? *N. Jb. Mineral. Abh.*, **147**, 47–57.

Downloaded from https://pubs.geoscienceworld.org/eurjmin/article-pdf/30/5/1021/4541283/ejm_30_5_1021_1035_biagioni_2765_online.pdf
by University of Arizona user

Kawada, I. & Hellner, E. (1971): Die Kristallstruktur der Pseudozell (subcell) von Andorite VI (Ramdohrite). *N. Jb. Miner. Abh.*, **147**, 47–57.

Kraus, W. & Nolze, G. (1996): PowderCell – a program for the representation and manipulation of crystal structures and calculation of the resulting X-ray powder patterns. *J. Appl. Crystallogr.*, **29**, 301–303.

Liu, H. & Chang, L.L.Y. (1994): The Mn isotype of andorite and uchucchacuaite. *Can. Mineral.*, **32**, 185–188.

Makovicky, E. & Karup-Møller, S. (1977a): Chemistry and crystallography of the lillianite homologous series. I. General properties and definitions. *N. Jb. Miner. Abh.*, **130**, 264–287.

—, — (1977b): Chemistry and crystallography of the lillianite homologous series. II. Definition of new minerals: eskimoite, vikingite, ourayite and treasurite. Redefinition of schirmerite and new data on the lillianite – gustavite solid-solutions series. *N. Jb. Miner. Abh.*, **131**, 56–82.

Makovicky, E. & Topa, D. (2011): The crystal structure of gustavite, $PbAgBi_3S_6$: analysis of twinning and polytypism using the OD approach. *Eur. J. Mineral.*, **23**, 537–550.

—, — (2014a): Lillianites and andorites: new life for the oldest homologous series of sulfosalts. *Mineral. Mag.*, **78**, 387–414.

—, — (2014b): The crystal structure of jasrouxite, a Pb-Ag-As-Sb member of the lillianite homologous series. *Eur. J. Mineral.*, **26**, 145–155.

Makovicky, E., Mumme, W.G., Gable, R.W. (2013): The crystal structure of ramdohrite, $Pb_{5.9}Fe_{0.1}Mn_{0.1}In_{0.1}Cd_{0.2}Ag_{2.8}Sb_{10.8}S_{24}$: a new refinement. *Am. Mineral.*, **98**, 773–779.

Makovicky, E., Stöger, B., Topa, D. (2018a): The incommensurately modulated structure of roshchinite, $Cu_{0.09}Ag_{1.04}Pb_{0.65}Sb_{2.82}As_{0.37}S_{6.08}$. *Z. Kristallogr.*, **233**, 255–268.

Makovicky, E., Topa, D., Paar, W.H. (2018b): The definition and crystal structure of clino-oscarkempffite, $Ag_{15}Pb_6Sb_{21}Bi_{18}S_{72}$. *Eur. J. Mineral.*, **30**, in press, DOI: 10.1127/ejm/2017/0029-2688.

Mantienne, J. (1974): La minéralisation thallifère de Jas Roux (Hautes Alpes). Doctorate thesis, Univ. Paris VI, 153 p.

Moëlo, Y., Makovicky, E., Karup-Møller, S. (1984): New data on the minerals of the andorite series. *N. Jb. Miner. Mh.*, **1989**, 175–182.

—, —, — (1989): Sulfures complexes plombo-argentifères: minéralogie et cristallochimie de la série andorite-fizelyite, $(Pb,Mn,Fe,Cd,Sn)_{3-2x}(Ag,Cu)_x(Sb,Bi,As)_{2+x}(S,Se)_6$. *Doc. BRGM*, **167**, 107 p.

Moëlo, Y., Makovicky, E., Mozgova, N.N., Jambor, J.L., Cook, N., Pring., A., Paar, W.H., Nickel, E.H., Graeser, S., Karup-Møller, S., Balić-Žunić, T., Mumme, W.G., Vurro, F., Topa, D., Bindi, L., Bente, K., Shimizu, M. (2008): Sulfosalt systematics: a review. Report of the sulfosalt sub-committee of the IMA Commission on Ore Mineralogy. *Eur. J. Mineral.*, **20**, 7–46.

Moëlo, Y., Guillot-Deudon, C., Evain, M., Orlandi, P., Biagioni, C. (2012): Comparative modular analysis of two complex sulfosalt structures: sterryite, $Cu(Ag,Cu)_3Pb_{19}(Sb,As)_{22}(As–As)S_{56}$, and parasterryite, $Ag_4Pb_{20}(Sb,As)_{24}S_{58}$. *Acta Crystallogr.*, **B68**, 480–492.

Mozgova, N.N., Bortnikov, N.S., Organova, N.I., Tsepin, A.I., Kuz'mina, O.V., Nekrasov, I. Ya. (1983): New data on the andorite homologous series. *Mineral. Zhurnal*, **5**, 17–33 (in Russian).

Mozgova, N.N., Nenasheva, S., Borodaev, Y., Sivtsov, A., Riabeva, E., Gamianin, G. (1987): New mineral varieties of the sulfosalt group. *Zap. Vser. Mineral. Obsh.*, **116**, 614–628 (in Russian).

Nespolo, M., Ozawa, T., Kawasaki, Y., Sugiyama, K. (2012): Structural relations and pseudosymmetries in the andorite homologous series. *J. Mineral. Petrol. Sci.*, **107**, 226–243.

Nuffield, E.W. (1945): Studies of mineral sulfosalts: X – Andorite, ramdohrite, fizelyite. *Trans. R. Soc. Canada*, **39**, 41–50.

Olsen, L.A., Balić-Žunić, T., Makovicky, E. (2008): High-pressure anisotropic distortion of $Pb_3Bi_2S_6$: a pressure-induced, reversible phase transition with migration of chemical bonds. *Inorg. Chem.*, **47**, 6756–6762.

Organova, N.I., Kuz'mina, O.V., Bortnikov, N.S., Mozgova, N.N. (1982): The crystal structure of the subcell of synthetic andorite-24. *Dokl. Akad. Nauk SSSR*, **267**, 939–942 (in Russian).

Orlandi, P. & Dini, A. (2004): Die Mineralien der Buca della Vena-Mine, Apuaner Berge, Toskana (Italien). *Lapis*, **29**, 11–24.

Orlandi, P., Dini, A., Olmi, F. (1998): Grumiplucite, a new mercury-bismuth sulfosalt species from the Levigliani mine, Apuan Alps, Tuscany, Italy. *Can. Mineral.*, **36**, 1321–1326.

Orlandi, P., Meerschaut, A., Moëlo, Y., Palvadeau, P., Léone, P. (2005): Lead-antimony sulfosalts from Tuscany (Italy). VIII. Rouxelite, $Cu_2HgPb_{22}Sb_{28}S_{64}(O,S)_2$, a new sulfosalt from Buca della Vena mine, Apuan Alps: definition and crystal structure. *Can. Mineral.*, **43**, 919–933.

Orlandi, P., Biagioni, C., Bonaccorsi, E., Moëlo, Y., Paar, W.H. (2012): Lead-antimony sulfosalts from Tuscany (Italy). XII. Boscardinite, $TlPb_4(Sb_7As_2)_{\Sigma 9}S_{18}$, a new mineral species from the Monte Arsiccio mine: occurrence and crystal structure. *Can. Mineral.*, **50**, 235–251.

Orlandi, P., Biagioni, C., Moëlo, Y., Bonaccorsi, E., Paar, W.H. (2013): Lead-antimony sulfosalts from Tuscany (Italy). XIII. Protochabournéite, $\sim Tl_2Pb(Sb_{9-8}As_{1-2})_{\Sigma 10}S_{17}$, from the Monte Arsiccio mine: occurrence, crystal structure and relationship with chabournéite. *Can. Mineral.*, **51**, 475–494.

Otto, H.H. & Strunz, H. (1968): Zur Kristallchemie synthetischer Blei-Wismut-Spießglanze. *N. Jb. Miner. Abh.*, **108**, 1–19.

Pažout, R. & Dušek, M. (2009): Natural monoclinic $AgPb(Bi_2Sb)_3S_6$, an Sb-rich gustavite. *Acta Crystallogr.*, **C65**, i77–i80.

Pinto, D., Balić-Žunić, T., Garavelli, A., Makovicky, E., Vurro, F. (2006): Comparative crystal-structure study of Ag-free lillianite and galenobismutite from Vulcano, Aeolian Islands, Italy. *Can. Mineral.*, **44**, 159–175.

Sawada, H., Kawada, I., Hellner, E., Tokonami, M. (1987): The crystal structure of senandorite (andorite VI): $PbAgSb_3S_6$. *Z. Kristallogr.*, **180**, 141–150.

Sheldrick, G.M. (2015): Crystal structure refinement with SHELXL. *Acta Crystallogr.*, **C71**, 3–8.

Spiridonov, E.M., Petrova, I.B., Dashevskaya, D.M., Balashov, H.E. (1990): Roshchinite – new mineral of the andorite group. *Zap. Vses. Mineral. Obsh.*, **119**, 32–43 (in Russian).

Sugaki, A., Shima, H., Kitakaze, A. (1974): Synthesize lead bismuth sulfosalts minerals: heyrovskyite, lillianite and galenobismutite (synthetic sulfide minerals (VI)). *Tech. Rep. Yamaguchi Univ.*, **1**, 360–368.

Takagi, J. & Takéuchi, Y. (1972): The crystal structure of lillianite. *Acta Crystallogr.*, **B28**, 649–651.

Downloaded from https://pubs.geoscienceworld.org/eurjmin/article-pdf/30/5/1021/4541283/ejm_30_5_1021_1035_biagioni_2765_online.pdf
by University of Arizona user

Topa, D., Makovicky, E., Putz, H., Zagler, G., Tajjedin, H. (2013a): Arsenquatrandorite, IMA 2012-087. CNMNC Newsletter No. 16, August 2013, page 2696. *Mineral. Mag.*, **77**, 2695–2709.

Topa, D., Makovicky, E., Favreau, G., Bourgoin, V., Boulliard, J.-C., Zagler, G., Putz, H. (2013b): Jasrouxite, a new Pb-Ag-As-Sb member of the lillianite homologous series from Jas Roux, Hautes-Alpes, France. *Eur. J. Mineral*., **25**, 1031–1038.

Topa, D., Paar, W.H., Makovicky, E., Stanley, C., Roberts, A.C. (2016): Oscarkempffite, $Ag_{10}Pb_4(Sb_{17}Bi_9)_{\Sigma 26}S_{48}$, a new Sb-Bi member of the lillianite homologous series. *Mineral. Mag*., **80**, 809–817.

Wilson, A.J.C., Ed. (1992): International Tables for Crystallography, Volume C: Mathematical, physical and chemical tables. Kluwer Academic, Dordrecht, NL.

Yang, H., Downs, R.T., Burt, J.B., Costin, G. (2009): Structure refinement of an untwinned single crystal of Ag-excess fizélyite, $Ag_{5.94}Pb_{13.74}Sb_{20.84}S_{48}$. *Can. Mineral.*, **47**, 1257–1264.

Yang, H., Downs, R.T., Evans, S.H., Feinglos, M.N., Tait, K.T. (2011): Crystal structure of uchucchacuaite, $AgMnPb_3Sb_5S_{12}$, and its relationship with ramdohrite and fizélyite. *Am. Mineral*., **96**, 1186–1189.

Yang, H., Downs, R.T., Evans, S.H., Pinch, W.W. (2013): Terrywallaceite, $AgPb(Sb,Bi)_3S_6$, isotypic with gustavite, a new mineral from Mina Herminia, Julcani Mining District, Huancavelica, Peru. *Am. Mineral*., **98**, 1310–1314.

Received 12 February 2018
Modified version received 31 March 2018
Accepted 11 April 2018

Downloaded from https://pubs.geoscienceworld.org/eurjmin/article-pdf/30/5/1021/4541283/ejm_30_5_1021_1035_biagioni_2765_online.pdf
by University of Arizona user